Geophysical Research Letters

RESEARCH LETTER
10.1029/2021GL096072

3D Joint Inversion of Scanning Magnetic Microscopy Data

Z. Pastore[1], P. Lelievre[2], S. A. McEnroe[1], and N. S. Church[1]

[1]Department of Geoscience and Petroleum, Norwegian University of Science and Technology, Trondheim, Norway, [2]Department of Mathematics and Computer Science, Mount Allison University, Sackville, NB, Canada

Key Points:

- Magnetic data and microscopic inspection indicate the main source of remanent magnetization is oxide exsolution lamellae in pyroxenes
- Simultaneous inversion of scanning magnetic microscopy data acquired above and below the sample indicate heterogeneous magnetization
- Magnetic inversion results are consistent with sample's bulk remanent magnetization measurements

Supporting Information:

Supporting Information may be found in the online version of this article.

Correspondence to:

Z. Pastore,
zeudiap@hotmail.com

Citation:

Pastore, Z., Lelievre, P., McEnroe, S. A., & Church, N. S. (2022). 3D joint inversion of scanning magnetic microscopy data. *Geophysical Research Letters*, *49*, e2021GL096072. https://doi.org/10.1029/2021GL096072

Received 7 SEP 2021
Accepted 21 DEC 2021

Author Contributions:

Conceptualization: Z. Pastore, P. Lelievre, S. A. McEnroe, N. S. Church
Data curation: Z. Pastore, P. Lelievre, S. A. McEnroe, N. S. Church
Formal analysis: Z. Pastore, P. Lelievre, S. A. McEnroe, N. S. Church
Funding acquisition: S. A. McEnroe
Investigation: Z. Pastore, P. Lelievre, S. A. McEnroe, N. S. Church
Methodology: Z. Pastore, P. Lelievre
Project Administration: Z. Pastore, S. A. McEnroe
Resources: S. A. McEnroe
Supervision: S. A. McEnroe, N. S. Church

Abstract Scanning magnetic microscopy (SMM) is a modern magnetometry technique that maps the magnetic anomalies resulting from small-scale variations of remanent magnetization within a sample. This information is vital to understand the origin of rock behavior in laboratory experiments and in larger scale magnetic surveys. To quantify the fine-scale remanent magnetization, we used 3D magnetic vector inversion to jointly invert SMM data collected both above and below a 5 mm-thick norite sample from the Bjerkreim-Sokndal layered intrusion in South Norway. The sample is from an area with a striking remanent aeromagnetic anomaly which shows a minimum of −13,000 nT below background in the high-resolution helicopter survey. Inversion results confirm bulk remanent magnetization measurements with calculated median magnetization intensities between 79 and 106 A/m and a strong preferred magnetization direction perpendicular to the slab plane. Furthermore, results indicate that the main source of natural remanent magnetization is in the pyroxenes.

Plain Language Summary Retrieving the small-scale variation of the magnetization of a rock sample helps to identify the mineral phases containing the magnetization, and to evaluate their relative contribution to total bulk magnetization. This information can be used to understand the magnetic history of a sample and its geological setting. Today, rock samples can be magnetically scanned in a laboratory using a scanning magnetic microscope. This microscope measures the magnetic field at closely spaced points in a plane less than 1 mm from the sample surface. The main challenge in interpreting these results is the incorporation of additional information about the sample to yield a robust, constrained and reliable model. Here, we applied a 3D magnetization vector inversion (a sophisticated imaging method) and incorporated constraints for testing different hypothesis. We found that the magnetization inversions fit the data accurately and lead to bulk properties estimates consistent with those reported by previous studies.

1. Introduction

Remanent magnetization is a major component of magnetic anomalies in the Bjerkreim-Sokndal (BKS) layered intrusion, in southwest Norway. The BKS lies in doubly plunging syncline and is composed of 6 mega-cyclic units (MCU) subdivided into a sequence of zones, defined by the presence or absence of certain index minerals (Wilson et al., 1996) which in turn control the magnetic properties of the rocks and the magnetic pattern (McEnroe et al., 1996, 2001). In general, the positive induced anomalies are observed over cumulates dominated by magnetite and Ti-rich ilmenite while negative remanent magnetic anomalies are over hemo-ilmenite rich cumulates (McEnroe et al., 2009). A clear example of the latter is the striking negative anomaly observed on the east limb of the Bjerkreim Lobe at Heskestad, with amplitude of −13,000 nT in a high-resolution helicopter survey acquired at 60 m above topography, and below −30,000 nT in ground magnetic surveys (McEnroe, Brown, et al., 2004, McEnroe, Skilbrei, et al., 2004).

Here, we investigated the fine-scale mineral magnetic properties of a sample from this area. The magnetic response of this sample is completely dominated by remanence. Traditional rock magnetic methods, used to investigate the magnetization in natural rock samples, are bulk measurements resulting from magnetic properties' average contributions from all sources in proximity of the sensor. Scanning magnetic microscopy (SMM) is a high-resolution mapping technique that allows us to characterize magnetic contributions of individual mineral phases (deGroot et al., 2018; Egli & Heller, 2000; Hankard et al., 2009; Oda et al., 2011; Pastore et al., 2018, 2019, 2021; Weiss et al., 2007, 2016). SMM generates a map of the magnetic field distribution over a planar surface of a rock sample with sub-millimeter resolution which can be used to attribute specific magnetic signals to the underlying mineralogy. This information is vital for a complete understanding of the bulk magnetic properties of natural samples; it can be used to obtain direct information about the magnetization sources, to investigate the stability of discrete sources' magnetization and to get insights into the magnetic history of the rock. We selected a 5 mm

Validation: Z. Pastore, P. Lelievre
Visualization: Z. Pastore, P. Lelievre, N. S. Church
Writing – original draft: Z. Pastore, P. Lelievre, S. A. McEnroe, N. S. Church
Writing – review & editing: Z. Pastore, P. Lelievre, S. A. McEnroe, N. S. Church

thick slice of the sample, rather than a petrographic thin section commonly used in SMM, to (a) minimize the contribution of particles at the cut surface, which can have their magnetization altered by the preparation process (Egli & Heller, 2000), and to (b) preserve the natural texture and microstructure (grain size and shape) of the mineral assemblage; the study sample is indeed a coarse-grained rock with major mineral phases in the mm-size.

To quantify the small-scale variation of the magnetization between and within grains, and further to verify the link between microstructure and magnetization, we employed state-of-the-art magnetic vector inversion (MVI) methods. The MVI problem suffers from a high degree of nonuniqueness and additional constraints are required to obtain accurate, reliable and interpretable results. To reduce degrees of freedom we incorporated geometrical constraints from optical images and simultaneously inverted SMM data collected above and below the sample, which is critical for improving depth resolution of magnetic sources. To assess if the SMM techniques and the inversion method used here can accurately characterize the contribution of individual particles or phases, we compared known bulk properties of the study sample with the modeled magnetization recovered from the magnetic inversions.

2. Materials and Methods

2.1. Petrography and Mineral Chemistry

The study sample is an ilmenite norite which belongs to the Megacyclic Unit IVe of the BKS layered intrusion. Electron microprobe element mapping of a companion slice of the sample shows that the dominant silicate phases are plagioclase and orthopyroxene with minor clinopyroxene and apatite. The discrete opaque phases are hemo-ilmenite and magnetite (Figure 1a). Exsolved opaques are common in the silicates: McEnroe, Skilbrei, et al. (2004) describe lamellae of hemo-ilmenite in the orthopyroxenes, and magnetite blades with ilmenite lamellae in the clinopyroxenes (Frandsen et al., 2004). McEnroe et al. (2000) and Robinson et al. (2001) describe the chemical and petrographic oxide phases in Unit IVe from Heskstad.

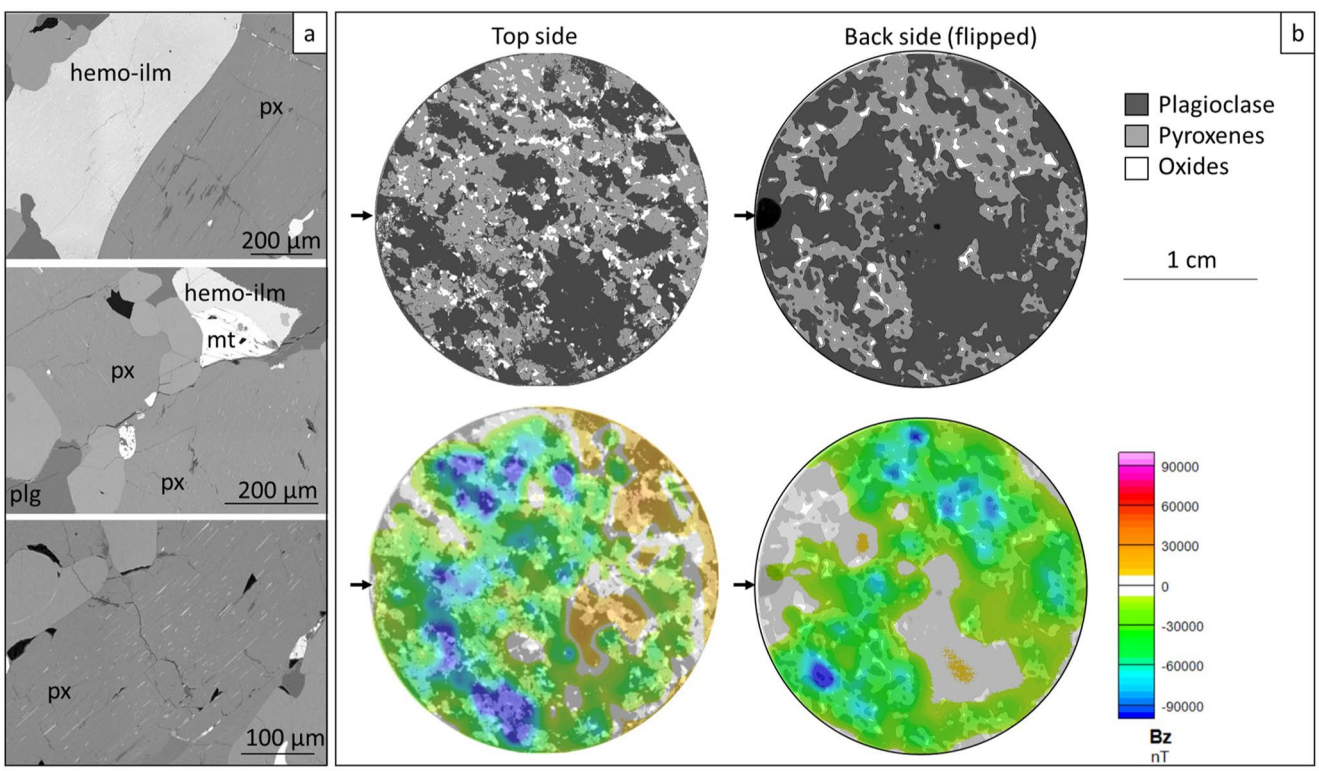

Figure 1. (a) Electron backscatterd images of a thin section made from the study sample. (b) Simplified mineralogy of top and bottom sides of the study sample slice (above) and overlays of respective top and bottom magnetic scans with the mineralogy (below). Note that images of the bottom have been flipped along the *y* axis and that Bz values for the top scan are reversed. The black arrows on the left side of the images of the core mark the orientation of the paleomagnetic core with reference to magnetic north.

The aim of this study is to investigate the source of the exceptionally high remanent magnetization of the study sample. Bulk magnetic measurements on the sample core have a natural remanent magnetization (NRM) value of 52 A/m, volume susceptibility of 0.098 SI and a Königsberger ratio, calculated as the ratio between the NRM and the induced magnetization (susceptibility × local magnetic field), of 13.3.

2.2. Scanning Magnetic Microscopy

SMM measures the magnetic field in a plane above the rock sample surface by rastering a small magnetic sensor very close to the polished surface. Magnetic scans were performed with a scanning magnetic tunnel junction (MTJ) device at the Norges Teknisk-Naturvitenskapelige Universitet (NTNU) Rock and Paleomagnetism laboratory (Church & McEnroe, 2018; Pastore et al., 2019). The instrument measures the vertical component of the field and all imaging is carried out at room temperature (~20°C). Helmholtz coils compensate for ambient magnetic fields, allowing for mapping of the magnetic remanence field. Here, measurements were taken both above and below the study sample at a nominal sampling step of 50 μm in x and y for the scan made above the sample slice and 35 μm for that made below the sample slice. The sampling rate was varied between measurements to maximize per-point averaging time to improve signal-to-noise of low-frequency signals, subject to available instrument time. Measurements were conducted with a sensor-to-sample distance of approximately 200 μm. The MTJ microscope has field noise of ~70 nT/$\sqrt{\text{Hz}}$ at 1 Hz and positioning accuracy of ~100 nm.

The magnetic data are shown in Figure 1b overlain on the optical image of the sample. For display purposes the magnetic data were gridded using a minimum curvature gridding algorithm, which is the smoothest possible surface to the data points (Briggs, 1974). For the gridding we used a cell size of one fourth of the data sample interval. Other parameters controlling grid accuracy and coverage setting are: (a) maximum number of iterations, set to 100, (b) tolerance required for each grid cell set to a default of 0.1% of the range of the data and (c) blanking distance, that is, how far the grid is extrapolated away from the nearest data point, set to 35 and 25 μm for top and bottom scan data respectively. The overlays show strong magnetic fields over pyroxenes, and weak signals over the plagioclase. Here, the magnetic field is generated by the remanent magnetization of the sample and its intensity ranges between −152.2 and 36.1 μT in the magnetic scan of the top of the slice, and between −103.7–12.5 μT in the magnetic scan of the back side of the sample slice.

2.3. Magnetic Vector Inversion (MVI)

To characterize the fine scale remanent magnetization of the thin section we used 3D magnetic vector inversion (MVI) of SMM data, using the methods of Lelièvre and Oldenburg (2009a). We discretized the volume of interest (the sample thin-section) into two types of meshes. First, a rectilinear mesh with equidimensional cells of dimension 500 μm was generated to fill a 25,500 μm by 25,500 μm by 5,000 μm rectangular prismatic volume. Any cells with centroids outside the cylindrical sample volume were removed for the purposes of inversion, leaving 20,250 cells representing the sample. Second, we used a workflow combining Triangle (Shewchuck, 1996) and TetGen (Si, 2015) to generate an unstructured tetrahedral mesh containing smaller cells close to the top and bottom sample surfaces and larger cells near the middle of the sample: tetrahedral face areas on the top and bottom sample surfaces were constrained to be at most 62,500 $\mu m^2 = 250 \times 250$ μm, consistent with the smallest spacing of the decimated SMM data we used for inversion; tetrahedral volumes were constrained to be at most 125,000,000 μm^3, corresponding to the volume of the cells in the rectilinear mesh. The resulting unstructured mesh contained 105,581 cells.

MVI recovers a 3D distribution of magnetization, with each mesh cell having a three-component magnetization with some intensity and direction. Allowing a 3-component vector magnetization greatly increases the non-uniqueness of the magnetic inverse problem. Our methodology applied various regularization options and constraints to explore the space of all possible models. To do so, we use a highly flexible and functional inversion software package, MAGNUM, developed jointly at Mount Allison University and Memorial University of Newfoundland, that allowed incorporation of all the constraints we were interested in.

We inverted using the Cartesian formulation of Lelièvre and Oldenburg (2009a), where the magnetization is defined as having three orthogonal components in some arbitrary reference frame. Initial inversions used the typical default smoothing regularization, effectively a sum-of-squares on the differences between magnetization components in adjacent mesh cells. This regularization approach generates models with smooth spatial gradients.

We used a sensitivity weighting approach to counteract the decay of the magnetic kernels, following Li & Oldenburg (2000), using the default parameter value $\beta = 1.0$ (see their equation 18).

Additional inversions were run with several different regularization options. Because the data are collected both above and below the sample, some experimentation was required to determine an appropriate value for the sensitivity weighting parameter β. For some inversions, we replaced the default smoothing regularization with a total-variation regularization, using an Ekblom measure with power $p = 1.1$ and $\epsilon = 10^{-6}$ to approximate the L1 norm: see Farquharson and Oldenburg (1998) and Galley et al. (2020). Use of total-variation regularization allows for sharper spatial changes in the magnetization across the inversion mesh, and is therefore more consistent with the fact that the sample is a collection of magnetic and non-magnetic grains. For other inversions, we used a smoothness regularization with rotated smoothness axis directions: see Li & Oldenburg (2020), Lelièvre and Oldenburg (2009b) and Lelièvre and Farquharson (2013). This allowed us to prescribe a preferential direction of smoothness along the plunge direction of the crystals of based on field measurements of lineation/foliation plunges and on previous electron backscatter diffraction measurements of minerals' crystallographic orientation (McEnroe, Skilbrei, et al., 2004). For the pyroxenes we considered a plunge of 72° and a plunge azimuth of 201°. This generates models with more continuous magnetization in that plunge direction but with sharper discontinuities perpendicular to that, for example, across crystal boundaries. Finally, additional inversions were performed that specified that the magnetization should be in the direction of the bulk remanent magnetization recovered from previous work (Brown & McEnroe, 2015; McEnroe, Skilbrei, et al., 2004, 2009): see Lelièvre and Oldenburg (2009a) for details on how this is achieved.

Other variables that we investigated included the mesh discretization (cell dimensions in the rectilinear mesh), the amount of data used (data decimation), and the level of data fitting. For the latter, we assigned uncertainties of 3,000 nT to the data measurements, which is about 1.6% of the range of data measurements (−152252–36,107 nT). This is an uncertainty estimate based on experience: usually a value between 1% and 5% of the data range is used. The choice is arbitrary because the actual fit to the data is controlled by the assigned target misfit. To assess an appropriate level of data fit we took the common approach of inverting at many different target misfits and performing a visual assessment of the recovered magnetization models and data residuals. Overfitting of the data was apparent in the recovered magnetization models as a clear increase in anomalous structure, particularly near the edges of the sample, and in the data residuals as spatially correlated features in the data misfit map. We also used the stats.normaltest function from the Python SciPy library to obtain a quantitative measure of the normality of the residual distributions, and the plotting.autocorrelation_plot function from the Python pandas library to assess the spatial correlation in the residuals. Together, these assessments suggested a target misfit in the range 0.5–2.0 was most appropriate.

All of these various inversions served to explore the space of all possible models for this non-unique MVI problem, but the resulting bulk magnetizations for all inversions were fairly constant (see Table S1 in the Supporting Information S1). The bulk magnetization is determined from a vector magnetization model by first calculating the volume-averaged Cartesian magnetization components. Those averaged Cartesian components are then converted to spherical coordinates to provide bulk magnetization amplitude, inclination and declination. Figure 2 shows the result of our MVI that was most consistent with the most accurate and verifiable a priori information; this MVI used the finest rectilinear mesh and data spacing possible for our computing platform, it applied total-variation regularization, and used sensitivity weighting with the default $\beta = 1.0$.

3. Results

Only minor variations were observed between the models recovered by inversion of the data. Model differences were assessed by comparing bulk magnetization properties and through directional data dispersion statistics (see Table S1 in the Supporting Information S1). All models show similar mean vector directions with angular standard deviations below 33.6°; however, a higher precision parameter ($k = 9.9$, Butler [1998]) and a lower angular standard deviation (25.7°) are estimated for model B. For display purposes we selected this model recovered with a total-variation regularization (Figure 2). As mentioned above, the latter allows for sharper spatial changes in the magnetization across the inversion mesh and is therefore more consistent with the fact that the sample is a collection of magnetic and non-magnetic grains. All other models are available in a repository at DataverseNO.

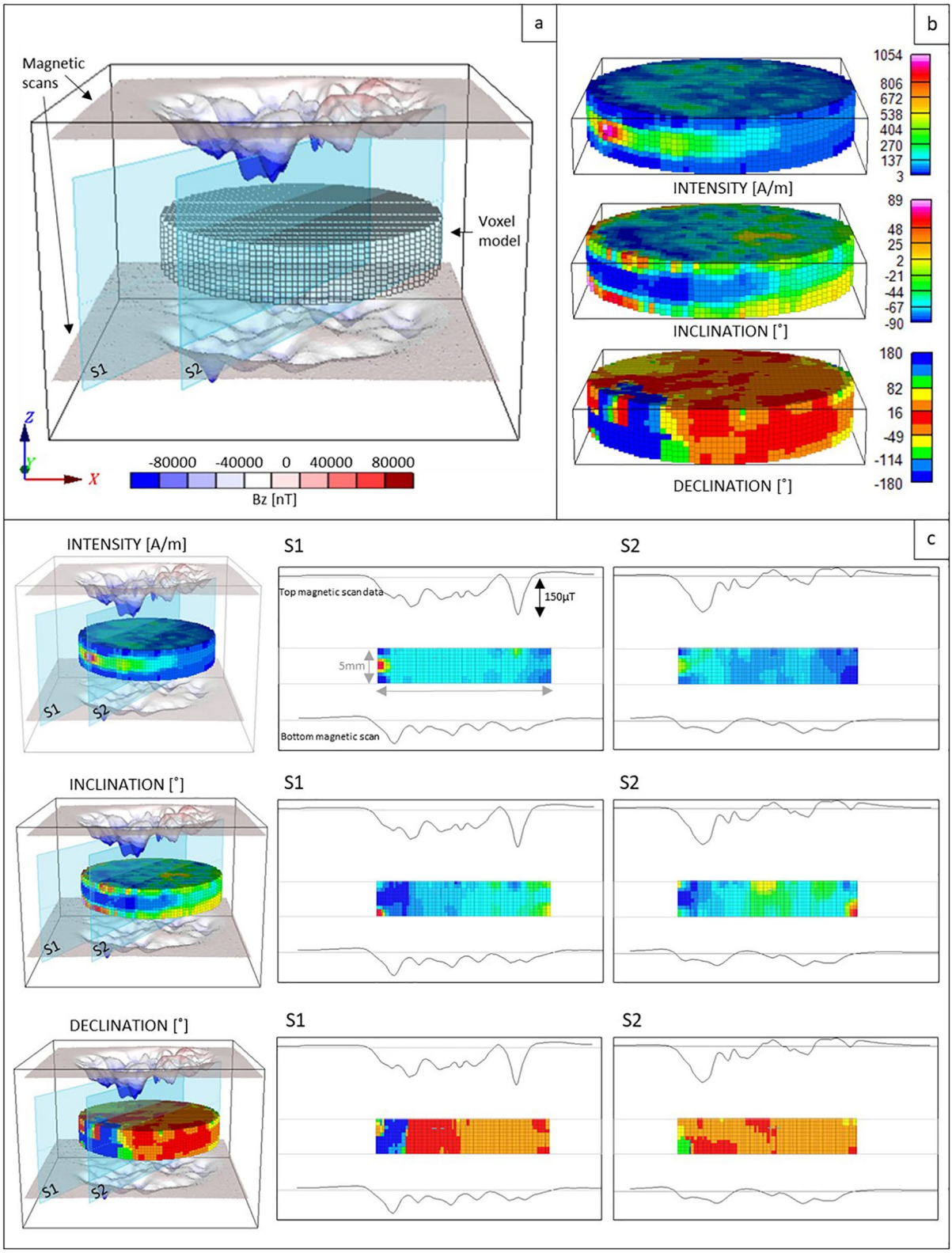

Figure 2. Perspective and cross-sections views of model B recovered with a total variation regularization by simultaneous inversion of top and bottom magnetic scan data. (a) Perspective view with surface magnetic grids from top and bottom magnetic scans and sample's voxel model in the middle. (b) Voxel-models colored by magnetization intensity, inclination and declination respectively. (c) Perspective view and cross-sections (S1 and S2) of the model colored by magnetization intensity, inclination and declination.

Perspective views of the model recovered with a total variation regularization highlight areas of high magnetization intensity and steep inclinations within the sample volume and specifically within the pyroxenes. However, changes in declination angles lack a clear correlation with changes in intensity and/or inclinations. The magnetization intensity ranges from 2.7 to 1,054.16 A/m with a mean value of 101.69 A/m and a standard deviation of 68.24 A/m. Inclination angles range from −89.93° to 89.14° with a mean of −56.83° and a standard deviation of 23.43. Declination angles range from 0° to 360° with mean of 305° and standard deviation of 75.9. Values are in the same coordinate system used for modeling of the data, with the *x*–*y* plane parallel to the sample surface and *z* positive upward. Declination angles are calculated assuming north parallel to the *x* axis, and considering the sample's mark of the geographic north as zero declination (see black arrows in Figure 1).

While Figure 2b indicates a layer of more highly magnetic material sandwiched between lower regions, this is not the case. The anomalous high intensity seen in Figure 2b is only on the very side of the model, only a couple cells thick, and is likely an edge effect or a drilling induced magnetization that could be investigated in future work.

Figure 3 shows perspective views of representative models obtained using different regularizations: a default regularization (model A) that generates a smooth model compared with that obtained with the total variation (model B), an alternative regularization that encourages continuous features in the plunging direction of the grains and sharper changes allowed perpendicular to that direction (model C) and a regularization that encourages recovered magnetization directions to align with the calculated bulk direction (model D). Beside small variations, all models show consistent bulk magnetization results independent of the regularization used or data decimation. However, total variation (model B) and constrained magnetization direction regularization (model D) show outliers with intensity values above 300 A/m (see histograms in Figure 3) compared to models obtained with other regularizations. Cells with these values are mostly observed at the edge of the sample and are likely the effect of an artifact of the inversion.

4. Discussion

Here, we inverted SMM data on a 5 mm thick sample slice to model the sample's magnetization. To constrain the results better we used a joint inversion of magnetic scan data collected above and below the sample slice. This work is the first, to the authors' knowledge, to successfully invert experimental SMM data collected above and below a sample, which is critical for improving imaging depth resolution on thicker samples.

To assess the accuracy of the inversions, modeled bulk magnetizations were compared to bulk measurements on the core from which the 5 mm slice was made, and the two 1-inch companion samples cut from the original paleomagnetic core. A stereoplot in Figure 4 shows the distribution of individual cell's magnetization values and the resulting average magnetization for model B with mean vector intensity of 95.38 A/m, steep negative inclination of −68° and declination of 331°.

The stereoplot shows a preferred orientation in the distribution of individual voxels directions which resemble the orientation of rods and blades of ilmenite with exsolved hematite within the orthopyroxenes, observed by optical and transmission electron microscopy in a previous study by McEnroe, Skilbrei, et al. (2004). Although the size of these rods and blades is below the resolution of the magnetic scan data, this consistency suggests that there is an obvious anisotropy in the magnetization direction which is visible also at the resolution scale of the magnetic scans.

Nonuniqueness of inverse problem can be significantly reduced using prior information, for example, observed mineral fabric, sparsity of opaque grains through sample and independent magnetic measurements. However, we observed that imposed constraints did not significantly affect the results. All models yielded results consistent with the bulk remanent magnetization measurements on the study sample; in unrotated sample coordinates, the magnetization inclination angles range from −64° to −68°, while declination angles range from 301° to 312° (see McEnroe et al., 2009 for site properties in geographic coordinates).

All models indicate a magnetization with variable intensity across the sample volume but a consistent direction. Local changes within the models were mostly observed at the edges of the sample.

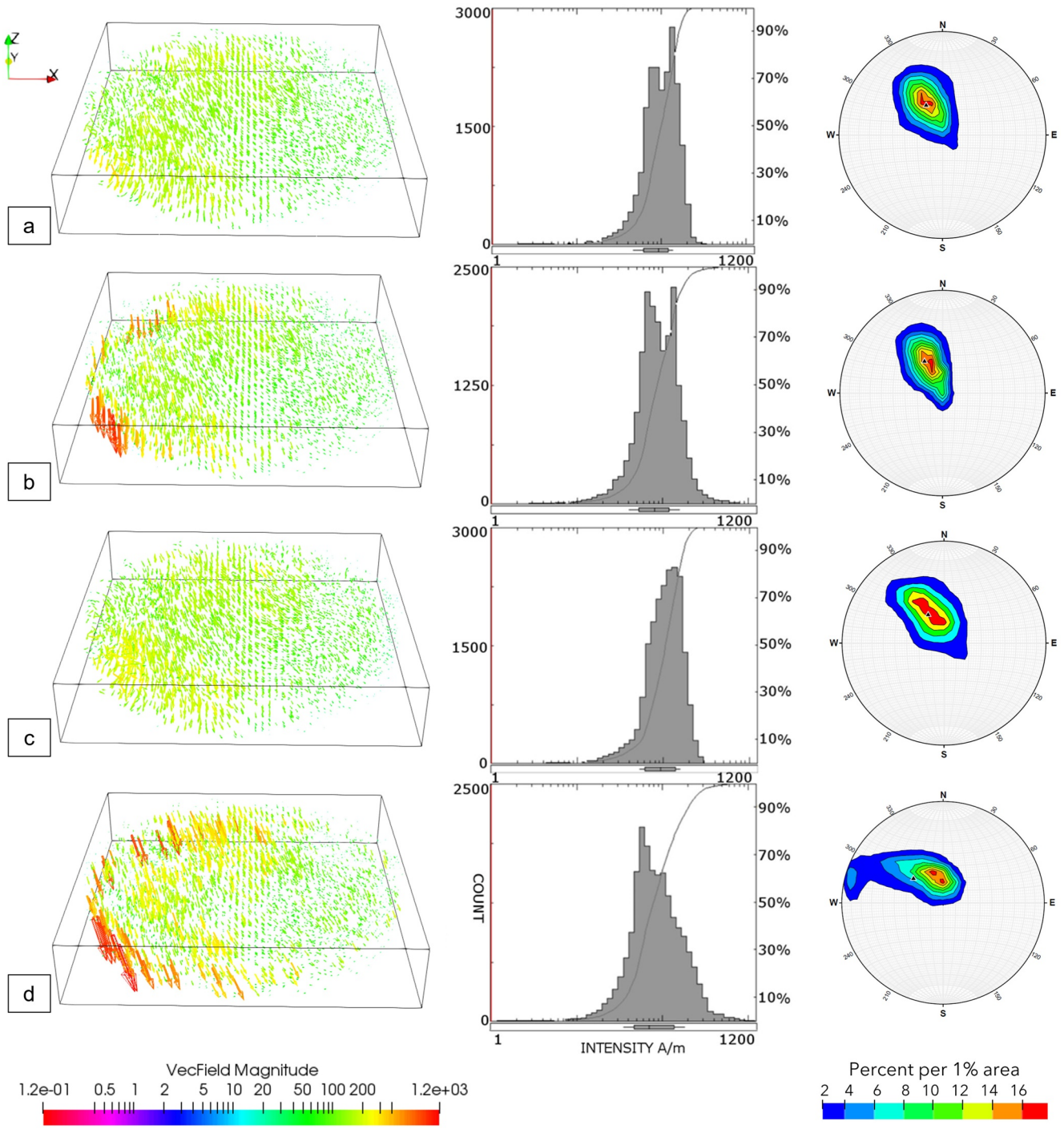

Figure 3. Left: Perspective views of representative models (see Table S1 in the Supporting Information S1 for differences in bulk magnetization calculations and dispersion statistics) with arrows indicating individual models' cells magnetization. Arrow orientation indicates the magnetization direction, and their color and size, the magnetization intensity in A/m. Middle: Histograms of magnetization intensity of models shown to the left in logarithmic scale (magnetization is shown in the horizontal axis and ranges from 0 to 1,200 A/m). Right: Stereonets with contour plots with a fixed counting circle at 1% area of individual voxels' directions for each of the models shown to the left.

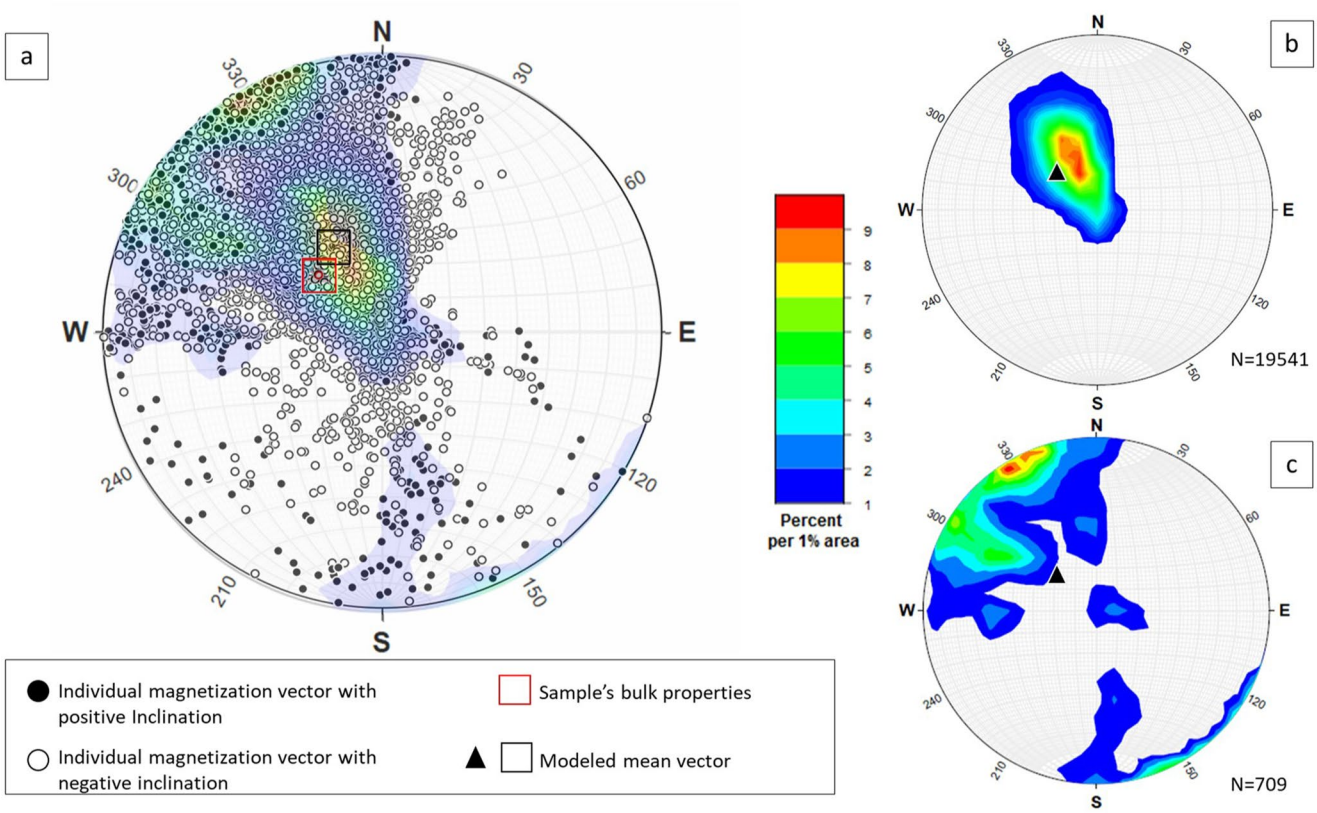

Figure 4. Stereoplot with data from model B. (a) Stereonet of discrete mesh cells magnetizations (open and closed circles) with overlayed in transparency contour plots of the same mesh cells shown in (b) and (c). The stereonet shows that the modeled mean vector calculated from all individual cells' magnetization is close to the expected bulk magnetization value measured on the core from which the investigated 5 mm slice was made (b) Contour plots of negative inclinations solutions with N indicating the number of vectors considered (19,541). (c) Contour plots of positive inclinations solutions with N indicating the number of vectors considered (709). Magnetization directions are given in sample coordinates considering the sample's mark (black arrow on the side of the sample image in Figure 1) as zero declination and z positive upward. Inclination angles indicate the magnetization orientation with respect to the x-y plane parallel to the sample surface. Closed circles indicate positive inclinations; open circles, negative inclinations.

5. Conclusions

Obtaining reliable information about the magnetic mineralogy of rock samples is vital for an understanding of the origin of rock bulk behavior in both the laboratory and larger scale magnetic surveys. Here, we used 3D magnetic vector inversion of SMM data to recover the small-scale remanent magnetization of a sample. We used various regularization options for hypothesis testing and these gave consistent results.

Our findings suggest that the magnetization intensity varies across the sample volume with areas of high intensity within the pyroxenes and a strong preferred magnetization direction perpendicular to the slab plane, as indicated by the steep inclination angles. This result is consistent with previous magnetic studies on this sample and companion norite specimens from this location.

The largest magnetization intensity is observed within the pyroxenes. This finding validates previous work indicating the exsolution in the pyroxenes are a main source of magnetization in this sample. These micron-sized exsolution lamellae have a large effect on the sample bulk property and consequently on the broad high-amplitude magnetic anomaly measured in the sampling region. However, a full understanding of the nature of the large remanent signal from the pyroxenes remains elusive and further transmission electron microscopy is planned to characterize these lamellae. Scanning magnetic microscopy is shown to be an excellent tool to investigate the sources of the magnetization at the mineral scale and to evaluate their contribution to the bulk rock properties, and to the correlative magnetic anomaly. This is an essential step to scale up interpretations from the mineral scale to the larger geological picture.

MVI has a potential for future detailed studies of remanent and induced magnetization with flexibility in incorporating constraints and testing various hypotheses. It has great potential to further our understanding of mineral magnetism, and with the application of magnetic fields of known intensity and directions using the Helmholtz coils, could greatly aid in developing our exploration tools.

Data Availability Statement

The magnetic data used to characterize the study sample's magnetization and results of magnetic simulations are available at dataverseNO via https://doi.org/10.18710/M5FSHT.

Acknowledgments
This research was supported by the Faculty of Engineering at NTNU. We greatly thank the reviewers Bill Morris and Ramon Egli for their constructive comments and their valuable suggestions, and the Editor Monika Korte. We dedicate this paper to Peter Robinson who provided deep insight into the magnetic behavior and chemistry of the oxide minerals studied here. His immense knowledge, kind encouragement and untiring energy is sorely missed.

References

Briggs, I. C. (1974). Machine contouring using minimum curvature. *Geophysics*, *39*(1), 39–48. https://doi.org/10.1190/1.1440410

Brown, L., & McEnroe, S. A. (2015). 916 Ma Pole for southwestern Baltica: Palaeomagnetism of the Bjerkreim-Sokndal layered intrusion, Rogaland Igneous Complex, southern Norway. *Geophysical Journal International*, *203*(1), 567–587. https://doi.org/10.1093/gji/ggv299

Butler, R. F. (1998). *Paleomagnetism: Magnetic domains to geological terranes*. Retrieved from https://websites.pmc.ucsc.edu/~njarboe/pmagresource/ButlerPaleomagnetismBook.pdf

Church, N. S., & McEnroe, S. A. (2018). Magnetic field surveys of thin sections. *Australian Society of Exploration Geophysicists Extended Abstracts*, *2018*(1), 1–5. https://doi.org/10.1071/ASEG2018abW10_3F

deGroot, L. V., Fabian, K., Béguin, A., Reith, P., Barnhoorn, A., & Hilgenkamp, H. (2018). Determining individual particle magnetizations in assemblages of micrograins. *Geophysical Research Letters*, *45*(7), 2995–3000. https://doi.org/10.1002/2017gl076634

Egli, R., & Heller, F. (2000). High-resolution imaging using a high-Tc superconducting quantum interference device (SQUID) magnetometer. *Journal of Geophysical Research: Solid Earth*, *105*(B11), 25709–25727. https://doi.org/10.1029/2000jb900192

Farquharson, C. G., & Oldenburg, D. W. (1998). Non-linear inversions using general measures of data misfit and model structure. *Geophysical Journal International*, *134*, 213–227. https://doi.org/10.1046/j.1365-246x.1998.00555.x

Frandsen, C., Stipp, S. L. S., McEnroe, S. A., Madsen, M. B., & Knudsen, J. M. (2004). Magnetic force microscopy (MFM) reveals magnetic domain structure and stray field of individual elongated magnetite grains. *Physics of the Earth and Planetary Interiors*, *141*, 121–129. https://doi.org/10.1016/j.pepi.2003.12.001

Galley, C. G., Jamieson, J. W., Lelièvre, P. G., Farquharson, C. G., & Parianos, J. M. (2020). Magnetic imaging of subseafloor hydrothermal fluid circulation pathways. *Science Advances*, *6*, eabc6844. https://doi.org/10.1126/sciadv.abc6844

Hankard, F., Gattacceca, J., Fermon, C., Pannetier-Lecoeur, M., Langlais, B., Quesnel, Y., et al. (2009). Magnetic field microscopy of rock samples using a giant magnetoresistance-based scanning magnetometer. *Geochemistry, Geophysics, Geosystems*, *10*(10), Q10Y06. https://doi.org/10.1029/2009GC002750

Lelièvre, P. G., & Farquharson, C. G. (2013). Gradient and smoothness regularization operators for geophysical inversion on unstructured meshes. *Geophysical Journal International*, *195*, 330–341.

Lelièvre, P. G., & Oldenburg, D. W. (2009a). A 3D total magnetization inversion applicable when significant, complicated remanence is present. *Geophysics*, *74*, L21–L30.

Lelièvre, P. G., & Oldenburg, D. W. (2009b). A comprehensive study of including structural orientation information in geophysical inversions. *Geophysical Journal International*, *178*, 623–637.

Li, Y., & Oldenburg, D. W. (2000). Joint inversion of surface and three-component borehole magnetic data. *Geophysics*, *65*, 540–552. https://doi.org/10.1190/1.1444749

Li, Y., & Oldenburg, D. W. (2020). Incorporating geological dip information into geophysical inversions. *Geophysics*, *65*, 148–157.

McEnroe, S. A., Brown, L. L., & Robinson, P. (2004). Earth analog for Martian magnetic anomalies: Remanence properties of hemo-ilmenite norites in the Bjerkreim-Sokndal Intrusion, Rogaland, Norway. *Journal of Applied Geophysics*, *56*(3), 195–212. https://doi.org/10.1016/s0926-9851(04)00052-7

McEnroe, S. A., Brown, L. L., & Robinson, P. (2009). Remanent and induced magnetic anomalies over a layered intrusion: Effects from crystal fractionation and magma recharge. *Tectonophysics*, *478*(1–2), 119–134. https://doi.org/10.1016/j.tecto.2008.11.021

McEnroe, S. A., Robinson, P., & Panish, P. T. (1996). Rock magnetic properties, oxide mineralogy, and mineral chemistry in relation to aeromagnetic interpretation and search for ilmenite reserves. *Norwegian Geological Survey Report*, *96*, 060.

McEnroe, S. A., Robinson, P., & Panish, P. T. (2000). Chemical and petrographic characterization of ilmenite-and magnetic-rich cumulates of the Sokndal Region, Rogaland, Norway. *Norwegian Geological Survey Bulletin*, *436*, 49–56.

McEnroe, S. A., Robinson, P., & Panish, P. T. (2001). Aeromagnetic anomalies, magnetic petrology and rock magnetism of hemo-ilmenite- and magnetite-rich cumulates from the Sokndal Region, South Rogaland, Norway. *American Mineralogist*, *86*(11–12), 1447–1468. https://doi.org/10.2138/am-2001-11-1213

McEnroe, S. A., Skilbrei, J. R., Robinson, P., Heidelbach, F., Langenhorst, F., & Brown, L. L. (2004). Magnetic anomalies, layered intrusions and Mars. *Geophysical Research Letters*, *31*, L19601. https://doi.org/10.1029/2004GL020640

Oda, H., Kawai, J., Miyamoto, M., Miyagi, I., Sato, M., Noguchi, A., et al. (2016). Scanning SQUID microscope system for geological samples: System integration and initial evaluation. *Earth Planets and Space*, *68*, 179. https://doi.org/10.1186/s40623-016-0549-3

Oda, H., Usui, A., Miyagi, I., Joshima, M., Weiss, B. P., Shantz, C., et al. (2011). Ultrafine-scale magnetostratigraphy of marine ferromanganese crust. *Geology*, *39*, 227–230. https://doi.org/10.1130/g31610.1

Pastore, Z., Church, N. S., & McEnroe, S. A. (2019). Multistep parametric inversion of scanning magnetic microscopy data for modeling magnetization of multidomain magnetite. *Geochemistry, Geophysics, Geosystems*, *20*, 5334–5351. https://doi.org/10.1029/2019GC008542

Pastore, Z., McEnroe, S. A., Church, N. S., & Oda, H. (2021). Mapping and modeling sources of natural remanent magnetization in the microcline–sillimanite gneiss, northwest Adirondack Mountains: Implications for crustal magnetism. *Geochemistry, Geophysics, Geosystems*, *22*, e2020GC009580. https://doi.org/10.1029/2020GC009580

Pastore, Z., McEnroe, S. A., ter Maat, G. W., Oda, H., Church, N. S., & Fumagalli, P. (2018). Mapping magnetic sources at the millimeter to micrometer scale in DUNITE and SERPENTINITE by high-resolution magnetic microscopy. *Lithos*, *323*, 174–190. https://doi.org/10.1016/j.lithos.2018.09.018

Robinson, P., Panish, P. T., & McEnroe, S. A. (2001). Minor element chemistry of hemo-ilmenite and magnetite in cumulate rocks from the Sokndal region, South Rogaland, Norway. *American Mineralogist*, *86*, 1469–1476. https://doi.org/10.2138/am-2001-11-1214

Shewchuck, J. R. (1996). Triangle: Engineering a 2D quality mesh generator and Delaunay triangulator. In M. C. Lin, & D. Manocha (Eds.), *Applied computational geometry: Towards geometric engineering. Lecture notes in computer science* (Vol. 1148, pp. 203–222). Springer-Verlag.

Si, H. (2015). TetGen, a delaunay-based quality tetrahedral mesh generator. *ACM Transactions on Mathematical Software*, *41*, 11. https://doi.org/10.1145/2629697

Weiss, B. P., Lima, E. A., Fong, L. E., & Baudenbacher, F. J. (2007). Paleomagnetic analysis using SQUID microscopy. *Journal of Geophysical Research*, *112*(B9), B09105. https://doi.org/10.1029/2007JB004940

Wilson, J. R., Robins, B., Nielsen, F. M., Duchesne, J. C., & Vander Auwera, J. (1996). The Bjerkreim-Sokndal layered intrusion, southwest Norway. In R. G. Cawthorn (Ed.), *Layered intrusions* (pp. 231–255). Elsevier Science. https://doi.org/10.1016/s0167-2894(96)80009-1